Thermochimica Acta, 125 (1988) 173–190
Elsevier Science Publishers B.V., Amsterdam – Printed in The Netherlands

STUDIES ON THE FORMATION OF γ-Fe_2O_3 BY THERMAL DECOMPOSITION OF FERROUS MALONATE DIHYDRATE

M.M. RAHMAN, V.A. MUKHEDKAR, A. VENKATARAMAN, A.K. NIKUMBH, S.B. KULKARNI * and A.J. MUKHEDKAR

Department of Chemistry, University of Poona, Pune 411 007 (India)

(Received 30 May 1987)

ABSTRACT

The thermal decomposition process of ferrous malonate dihydrate ($FeC_3H_2O_4 \cdot 2H_2O$) was studied in atmospheres of static air, dynamic dry nitrogen, dynamic dry air, and dynamic air containing water vapour by means of thermal analysis (simultaneous TGA, DTG and DTA), direct current electrical conductivity measurements, infrared spectroscopy, elemental analysis, gas–liquid chromatography and X-ray powder diffraction analysis. The conductivity data in static air and dynamic air are quite complex: nevertheless, the formation of Fe_3O_4 and α-Fe_2O_3 with the probable intermediate formation of γ-Fe_2O_3 has been indicated. In dry nitrogen the step corresponding to dehydration is well resolved in the temperature region 190–260 °C and the formation of FeO and Fe_3O_4 is also well characterised. A definite indication from the conductivity measurements for the formation of γ-Fe_2O_3 prior to α-Fe_2O_3 was found in an atmosphere of dynamic air containing water vapour. Experimental conditions were determined for the formation of γ-Fe_2O_3 in dynamic air containing water vapour. This compound (γ-Fe_2O_3) was characterised by X-ray diffraction, magnetic hysteresis, scanning electron microscopy and Mössbauer spectroscopy.

INTRODUCTION

Thermal decomposition studies of iron(II) carboxylates have become important research projects in the preparation of gamma ferric oxide (γ-Fe_2O_3) due to its application in magnetic recording tapes [1,2] and ferrite components. The usual method of preparation of γ-Fe_2O_3 is by reduction of α-Fe_2O_3 (obtained by dehydration of α-FeO(OH)) to Fe_3O_4 and reoxidation to γ-Fe_2O_3 [3]. There are reports on the preparation of γ-Fe_2O_3 from iron(II) carboxylate by using iron(II) oxalate dihydrate [4–7]. Another method for the synthesis of γ-Fe_2O_3 from thermal decomposition of ferrous oxalate dihydrate using direct current electrical conductivity for characterisation has been reported [8,9]. Recently the syntheses of γ-Fe_2O_3 by the thermal decomposition of ferrous fumarate [10] and ferrous succinate [11]

* Author to whom correspondence should be sent.

0040-6031/88/$03.50

have been reported. Though the thermal decomposition of ferrous malonate in an inert atmosphere has been reported [12], no systematic study has been undertaken for the characterisation of intermediates. In the present work, the thermal decomposition of ferrous malonate dihydrate has been studied using two-probe direct current electrical conductivity to investigate the conditions for the preparation of γ-Fe_2O_3. This study has been supplemented with TGA, DTG and DTA, X-ray diffraction, infrared spectroscopy and gas–liquid chromatography.

EXPERIMENTAL

Preparation of $FeC_3H_2O_4 \cdot 2H_2O$

Ferrous malonate dihydrate ($FeC_3H_2O_4 \cdot 2H_2O$) was prepared by dissolving ferrous carbonate in an aqueous solution of malonic acid (10% excess) at 70 °C under a dynamic (pure and dry) nitrogen atmosphere [12]. The

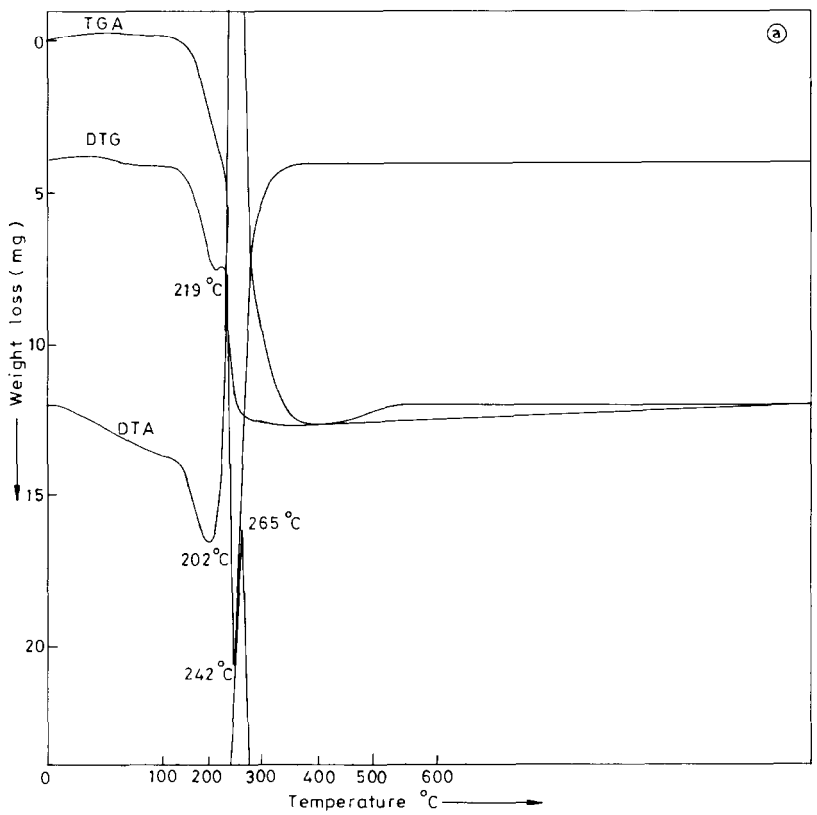

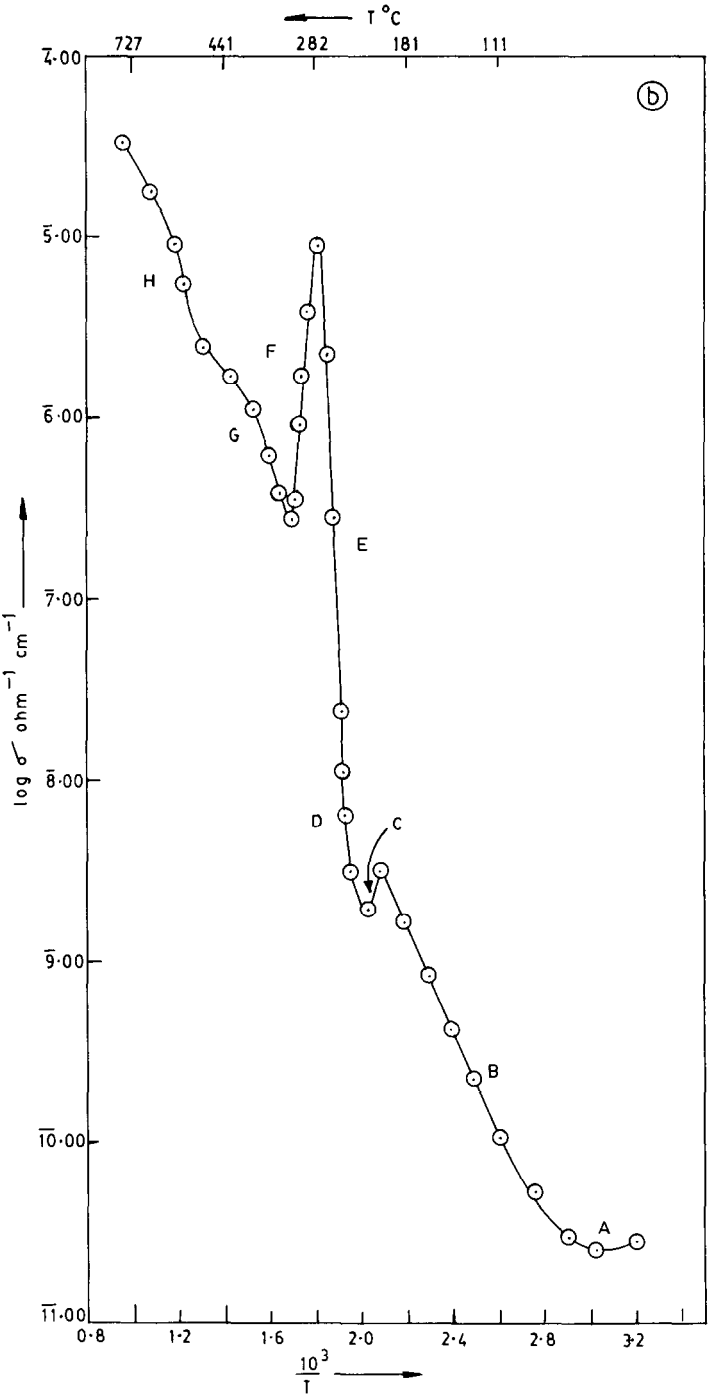

Fig. 1. Static air atmosphere (a) TGA, DTA and DTG curves for $FeC_3H_2O_4 \cdot 2H_2O$ (b) Plot of log σ vs. $1/T$ for $FeC_3H_2O_4 \cdot 2H_2O$.

elemental analysis was made for C, H and Fe [C, 18.77 (18.58); H, 3.10 (3.12); Fe, 28.65 (28.80)] where the values in parentheses are calculated ones.

The thermal analysis curves were obtained with a Netzsch instrument in an atmosphere of dynamic dry nitrogen, dynamic dry air (flowing at the rate of 100 ml min^{-1}) and static air in the temperature range of ambient to 1000 °C with a heating rate of 10 °C min^{-1}. The two-probe d.c. electrical conductivity (apparatus fabricated in the department) was measured on a Philips microvoltmeter PP 9004 instrument under static air, dynamic dry air, dynamic dry nitrogen and dynamic air containing water vapour [8]. The heating rate was adjusted to 10 °C min^{-1} and the flow rate for different atmospheres was maintained at 100 ml min^{-1}. The evolution of various gases during the thermal decomposition was recorded on Shimadzu Ria and Hewlett Packard instruments using nitrogen as the carrier gas. Infrared spectra were recorded on a Perkin–Elmer Model 337 spectrophotometer using nujol mull. The powder X-ray diffraction results were obtained on a PW 1730 Philips X-ray diffractometer using Fe K_α radiation.

The morphology of γ-Fe_2O_3 particles was investigated using a Cambridge Steroscan 150 instrument. The magnetic properties were studied using an alternating electromagnet type hysteresis loop tracer [12]. The Mössbauer spectra were obtained with a constant acceleration spectrometer coupled with a multichannel analyser assembled in the University Department of Physics.

RESULTS AND DISCUSSION

Static air atmosphere

The TGA, DTG and DTA curves for $FeC_3H_2O_4 \cdot 2H_2O$ are shown in Fig. 1(a). The dehydration of $FeC_3H_2O_4 \cdot 2H_2O$ was shown by an endothermic peak on the DTA curve at 202 °C and on the DTG curve at 219 °C. However the TGA curve showed a continuous weight loss between 128 and 265 °C indicating that the anhydrous malonate ($FeC_3H_2O_4$), formed at this temperature, is unstable. A sharp exothermic peak (at 265 °C) between 220 and 379 °C on the DTA curve and also a sharp endothermic peak (at 242 °C) between 230 and 379 °C on the DTG curve, corresponding to the oxidative decomposition of $FeC_3H_2O_4$ to poorly crystallised α-Fe_2O_3, were noted.

A comparison of conventional thermal analysis with conductivity analysis shows that the conductivity analysis gives a much more detailed view of the decomposition process. The temperature variation of electrical conductivity σ Fig. 1(b) does not show much change with the variation of temperature from 27 to 65 °C (Region A). There was a steady increase in the value of σ between 65 and 203 °C (Region B) followed by a linear decrease between 203 and 217 °C (Region C). A steep increase was observed between 220 and

245 °C (Region D), then there was a sudden increase in σ at 255 °C giving a maximum at 282 °C (Region E). There then was a linear decrease in σ between 282 and 315 °C (Region F), and then the value of σ rose in the range 315–440 °C (Region G) giving a definite shoulder at 475 °C, and finally increased linearly from 500 °C (Region H).

The plot of log σ vs. T^{-1} showed that the decomposition of $FeC_3H_2O_4 \cdot 2H_2O$ proceeds with the formation of the intermediates having different conductivity values, whereas in conventional thermal analysis the TGA curve showed a continuous weight loss, and the DTA curve showed only one sharp exothermic peak corresponding to oxidative decomposition.

The analysis of the log σ vs. T^{-1} plot must give due consideration to the physical factors involved in transforming a compound (formed during a chemical reaction) in the amorphous phase of fusion layers to large crystallites through the probable transformations, such as the formation of a fine network of grain boundaries and subsequent consolidation, and the formation of defects and subsequent annealing of such defects. It is therefore necessary to supplement the electrical conductivity measurements with other measurements of the structural characteristics of the samples, such as measurements of the IR spectra and the X-ray diffraction patterns.

In Region A of Fig. 1(b) there was no observable change in the X-ray diffraction pattern and IR spectrum for the sample heated isothermally. In the temperature range corresponding to Region B in Fig. 1(b), the IR spectrum showed sharp peaks for the malonate group frequencies [13] and the H–OH band decreased in intensity. The X-ray diffraction pattern also showed broad peaks with no observable change. A sample heated isothermally (at 210 °C) in Region C of Fig. 1(b) showed no H–OH bands in the IR spectrum; however the XRD pattern was less crystalline [14] with a slight decrease in the interplanar spacings. The elemental analysis also agreed well for anhydrous malonate ($FeC_3H_2O_4$). This Region C corresponded to the dehydration step for $FeC_3H_2O_4 \cdot 2H_2O$ [15]. The isothermally heated $FeC_3H_2O_4 \cdot 2H_2O$ sample in Region D showed large changes. The IR spectrum of the sample heated at 240 °C did not show any bands corresponding to the malonate group, but a strong and broad band at 550 cm^{-1} was observed. This band may be tentatively assigned to the Fe–O stretching mode in iron oxide [16]. The sample heated at 240 °C showed a complex X-ray diffraction pattern, probably a mixture of FeO, Fe_3O_4 and γ-Fe_2O_3. Thus the steep increase in conductivity observed in Region D in Fig. 1(b) was due to the transformation of $FeC_3H_2O_4$ to Fe_3O_4 possibly through the semiconducting FeO. In this experiment a separate step for the formation of FeO could not be identified. It should be noted here that the conductivity measurements were made on a dynamic system, while the other data was taken on samples obtained by isothermal heating at a specified temperature.

Although a tendency for a sharp increase in σ was observed at 255 °C the

characteristic high σ value for Fe_3O_4 ($\approx 10^{-3}$ ohm^{-1} cm^{-1}) could not be obtained under dynamic conditions and a decrease in the value of σ was seen at 282°C [Region F of Fig. 1(b)], probably due to the formation of semiconducting γ-Fe_2O_3. A sample in Region E in Fig. 1(b) was probably a mixture of Fe_3O_4 and γ-Fe_2O_3; the X-ray diffraction pattern was generally broad.

The X-ray diffraction pattern of a sample obtained from Region G showed that it was predominantly γ-Fe_2O_3 containing a small impurity of α-Fe_2O_3. A shoulder at 475°C just after Region G corresponded to the transformation of γ-Fe_2O_3 to α-Fe_2O_3. Thus the conductivity measurements supplemented with IR spectral data, X-ray diffraction pattern data and elemental analysis, gave a detailed analysis of the thermal decomposition of $FeC_3H_2O_4 \cdot 2H_2O$.

When the reaction was carried out using the static atmosphere, the gaseous product acted as a gas buffer for the solid-state reactions and some of the reactions were ill-defined. For example the role of water molecules in $FeC_3H_2O_4$ and the role of atmospheric oxygen in the solid-state reaction carried out in static air could be clarified by comparing the data of different physical properties for the reaction carried out in a dynamic dry nitrogen atmosphere.

Dynamic nitrogen atmosphere

The TGA curve of Fe(malonate)$\cdot 2H_2O$ [Fig. 2(a)] showed that this compound decomposed in three steps. The first step in the temperature range 121–254°C corresponded to complete dehydration [15]. The observed weight loss (18.03%) was in good agreement with the calculated value (18.57%). The DTA and DTG curves also showed well-defined peaks at 190 and 202°C, respectively, in the 121–254°C temperature range.

The temperature variation of electrical conductivity σ [Fig. 2(b)] initially showed a steady increase with a peak at 190°C (Region A). The isothermally heated sample of $FeC_3H_2O_4 \cdot 2H_2O$ in this region showed no observable change in the IR spectrum and X-ray diffraction pattern. Then there was a linear decrease in values of σ between 190 and 260°C (Region B). The sample obtained in this region showed no H–OH bands in the IR spectrum. Elemental analysis agreed well with the anhydrous compound $FeC_3H_2O_4$ and the X-ray diffraction pattern was less crystalline than the parent compound $FeC_3H_2O_4 \cdot 2H_2O$ (Table 1). Region B, therefore, corresponded to the dehydration of $FeC_3H_2O_4 \cdot 2H_2O$. The second step on the TGA curve in the temperature range 254–400°C corresponded to the decomposition of $FeC_3H_2O_4$. The observed weight loss (42.93%) was a little less than the calculated one (44.36%) for the formation of FeO. The DTA curve showed a broad peak at 309°C and the DTG curve at 320°C in the temperature range 254–400°C. The plot of log σ vs. $1/T$ [Fig. 2(b)] showed a steady

TABLE 1

X-ray diffraction data of $FeC_3H_2O_4 \cdot 2H_2O$

Observed *d*-spacing values (Å)	Observed *d*-spacing values (Å)	Observed *d*-spacing values (Å)
5.24(w)	2.73(s)	2.00(m)
4.72(s)	2.63(m)	1.93(s)
4.60(w)	2.50(s)	1.84(w)
4.15(s)	2.39(m)	1.80(w)
3.96(w)	2.38(s)	1.75(m)
3.65(m)	2.27(m)	1.69(m)
3.60(m)	2.24(m)	1.58(m)
3.15(m)	2.16(m)	1.43(s)
3.12(m)	2.08(m)	1.38(m)
2.89(s)	2.03(s)	

increase in values of σ in the temperature range 260–315 °C (Region C). A sample heated isothermally in this region showed that the IR bands attributable to Fe–O stretching frequencies became more intense and those due to co-ordinated carboxylate decreased in intensity. The X-ray diffraction pattern (Table 2) showed sharp lines indicating that the sample is predomi-

TABLE 2

X-ray diffraction data of $FeC_3H_2O_4$ and FeO obtained from $FeC_3H_2O_4 \cdot 2H_2O$ by heating under nitrogen atmosphere at 300 °C

Observed *d*-spacing values (present study) (Å)	FeO (cubic) *d*-spacing values [17] (Å)	FeO (rhombohedron) *d*-spacing values [19] (Å)
4.73(s)		
2.952(m)		
2.916(m)		
2.500(s)	2.49(80) [a]	
2.340(m)		
2.233(m)		
2.153(s)	2.153(100)	
2.090(m)		
2.026(s)		
1.970(w)		
1.708(w)		
1.613(m)		
1.605(m)		
1.518(m)	1.523(60)	1.525(100) [a]
1.300(w)	1.299(25)	1.301(20)
		1.236(60)
1.077(w)	1.077(15)	1.074(60)

[a] Figures in parentheses show the relative intensities normalised to that of the strongest intensity line (given by 100).

nantly crystalline. The pattern fits with the data for anhydrous ferrous malonate and cubic ferrous oxide [17]. The third step on the TGA curve showed weight loss in the temperature range 400–780 °C. The DTA and DTG curves showed an endothermic peak at 770 °C. However the weight loss calculated for the TGA curve did not reveal the formation of any single species.

A steep increase in σ was observed at 315 °C [Region D between 315 and 350 °C, Fig. 2(b)]. The sample obtained by heating isothermally in dry nitrogen at 420 °C showed a negligible variation in σ with variation of temperature. This behaviour is characteristic of Fe_3O_4 [20–22]. X-ray diffraction pattern data showed sharp lines and were comparable with the data reported for Fe_3O_4 [18] (Table 3). Thus the X-ray diffraction pattern, the temperature independence of σ and the magnetic properties (similar to those reported) suggest that the product obtained by the thermal decomposition of $FeC_3H_2O_4 \cdot 2H_2O$ under dynamic dry nitrogen at 420 °C is pure Fe_3O_4.

Comparison of the solid-state thermal decomposition reactions of $FeC_3H_2O_4 \cdot 2H_2O$ in normal static air and in dynamic dry nitrogen showed the following main differences:

(1) Malonate was unstable in static air, stable up to 260 °C in dry nitrogen, and intimately associated with the decomposed product up to 350 °C.

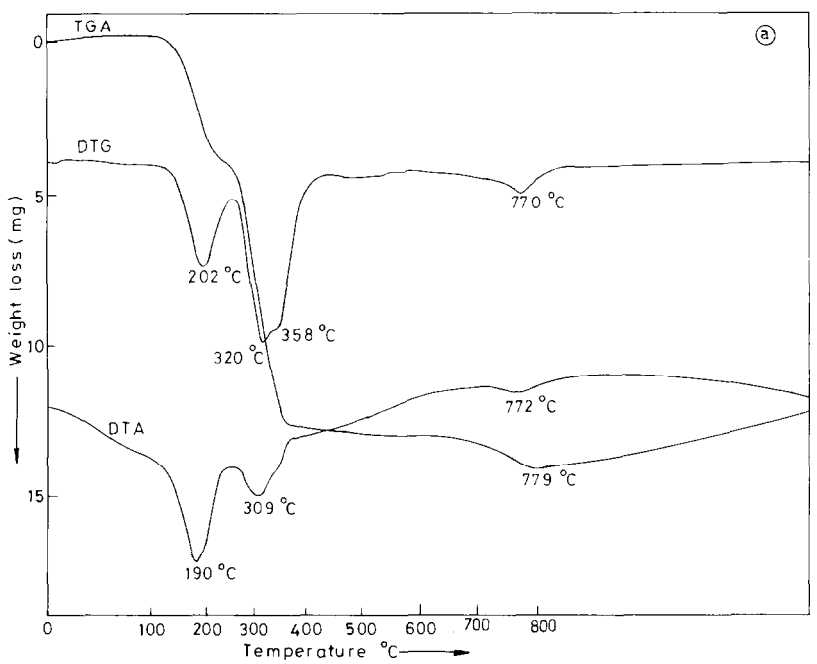

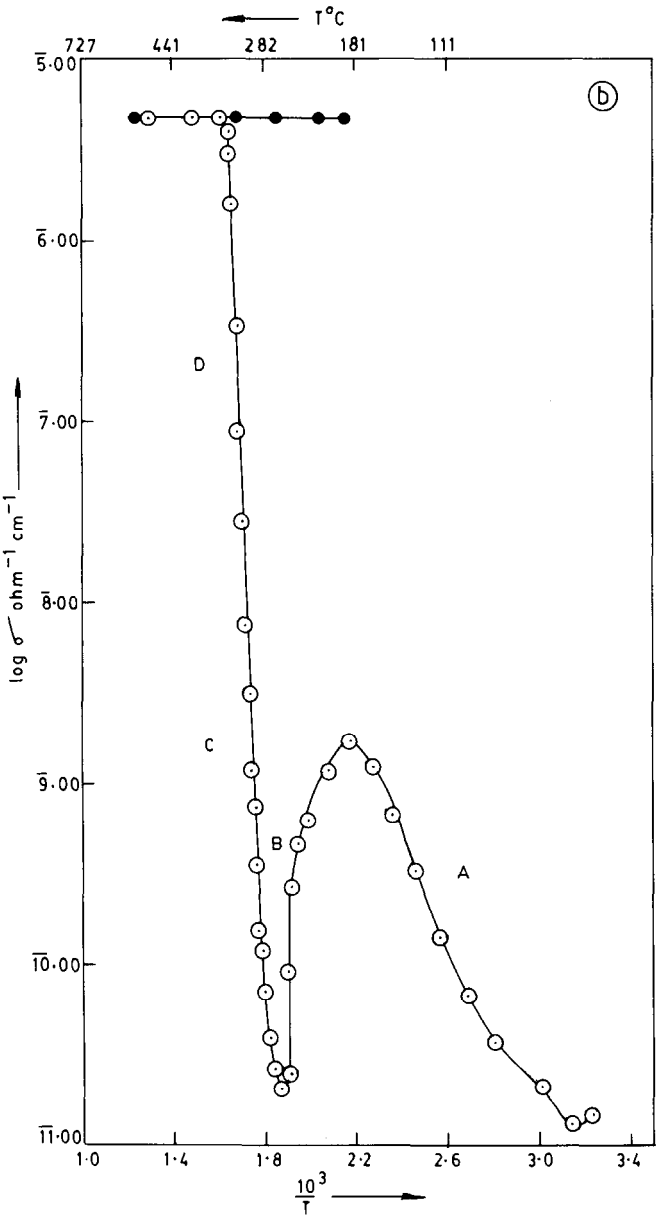

Fig. 2. Dynamic nitrogen atmosphere (a) TGA, DTA and DTG curves for $FeC_3H_2O_4 \cdot 2H_2O$. (b) Plot of log σ vs. $1/T$ for $FeC_3H_2O_4 \cdot 2H_2O$.

(2) The TGA curve under dynamic dry nitrogen showed a clear weight loss corresponding to the dehydration step, whereas a continuous weight loss was exhibited by the TGA curve under static air.

(3) The formation of the intermediate γ-Fe_2O_3 was indicated in the plots

TABLE 3

XRD data of Fe_3O_4 obtained from $FeC_3H_2O_4 \cdot 2H_2O$ by heating under nitrogen atmosphere at 450 °C

Observed *d*-spacing values (present study) (Å)	Fe_3O_4 *d*-spacing values [18] (Å)
4.87(w)	4.85(8) [a]
2.96(m)	2.967(30)
2.531(s)	2.532(100)
2.422(w)	2.424(8)
2.099(m)	2.099(20)
1.710(w)	1.715(10)
1.608(m)	1.616(30)
1.478(m)	1.485(40)
	1.419(2)
	1.328(4)
1.277(w)	1.281(10)
	1.266(4)
	1.212(2)
	1.122(4)
1.091(w)	1.093(12)
1.052(w)	1.050(6)

[a] Figures in parentheses show the relative intensities normalised to that of the strongest intensity line (given by 100).

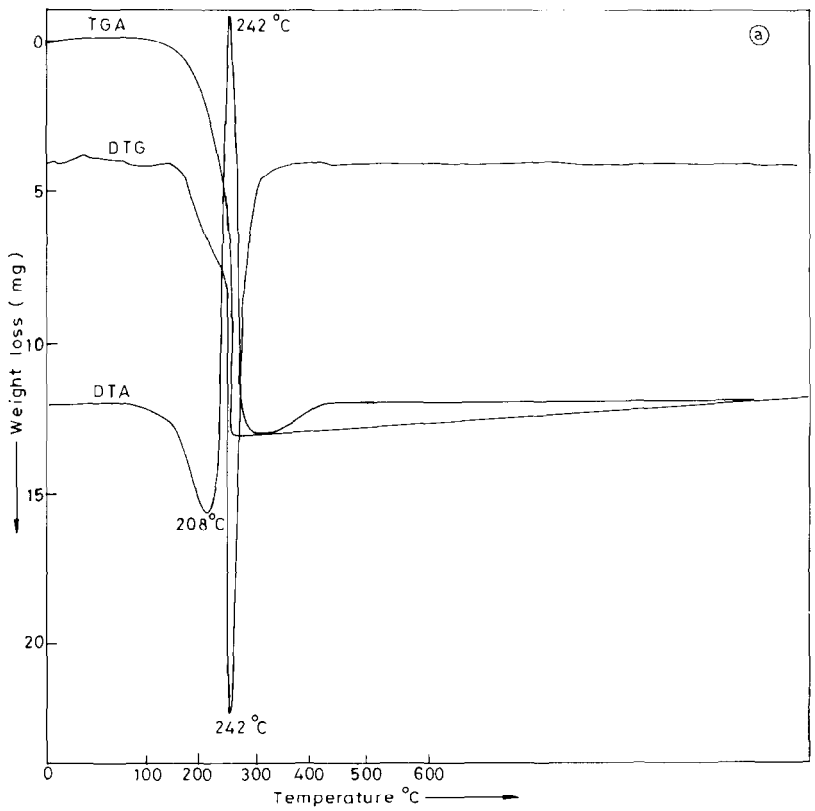

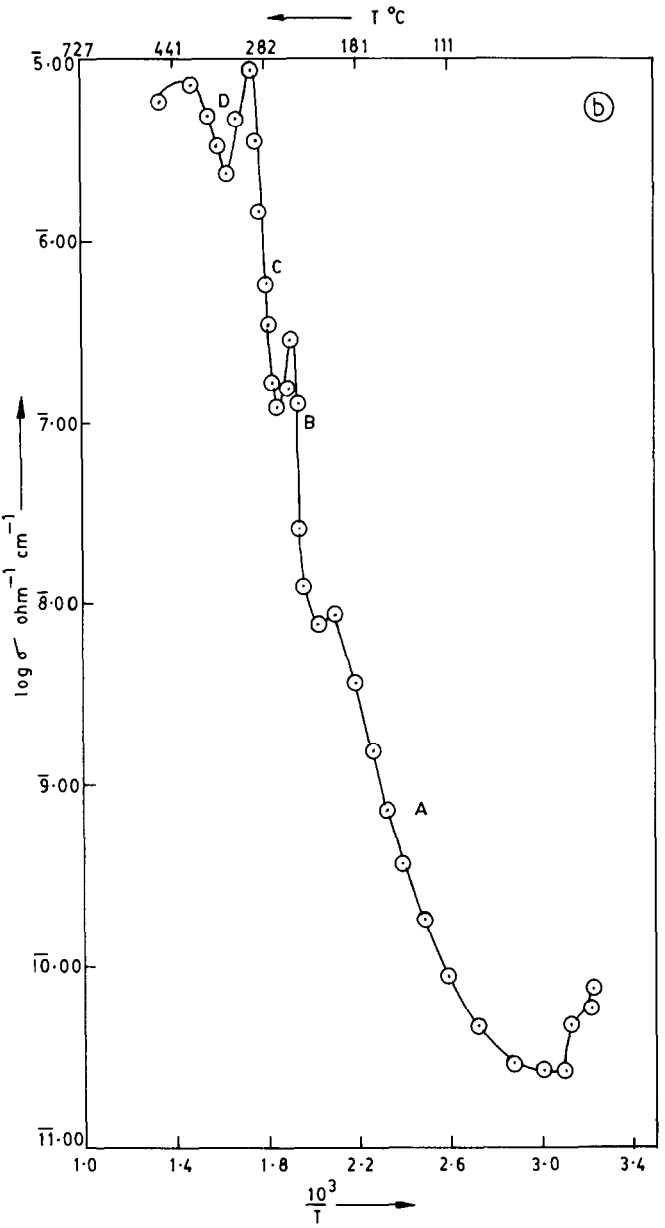

Fig. 3. Dynamic air atmosphere (a) TGA, DTA and DTG curves for $FeC_3H_2O_4 \cdot 2H_2O$ (b) Plot of log σ vs. $1/T$ for $FeC_3H_2O_4 \cdot 2H_2O$.

of log σ vs. $1/T$ in static air, but in dry nitrogen it could not be detected.

Since the nature of the solid-state decomposition of $FeC_3H_2O_4 \cdot 2H_2O$ is influenced by the composition of the atmosphere, it was considered advantageous to undertake similar measurements in other controlled atmospheres.

Dynamic air atmosphere

The TGA curve showed a continuous weight loss between 87 and 304 °C [Fig. 3(a)]. The DTG curve showed a broad peak at 242 °C. The DTA curve showed an endothermic peak at 208 °C corresponding to the dehydration of $FeC_3H_2O_4 \cdot 2H_2O$ and an exothermic peak at 242 °C corresponding to oxidative decomposition.

The plots of log σ vs. $1/T$ [Fig. 3(b)] showed a peak at 215 °C corresponding to the dehydration of $FeC_3H_2O_4 \cdot 2H_2O$. The sample heated isothermally in Region A at 220 °C showed no H–OH bands in the IR spectrum. The sample was crystalline to XRD. There was a steep increase in the value of σ between 235 and 250 °C (Region B), then there was a decrease and steep increase in values of σ in the temperature range 250–300 °C (Region C). These two temperature ranges, i.e. 235–250 and 250–300 °C, were tentatively assigned to the formation of FeO and Fe_3O_4 respectively. However repeated experiments to obtain pure FeO by careful heating in dynamic air always lead to the formation of a mixture of FeO and Fe_3O_4 (Table 4) [17–19]. X-ray diffraction patterns of the sample obtained showed broad lines revealing the product to be less crystalline. There was a sharp decrease and then an increase in values of σ between 300 and 390 °C (Region D). The X-ray diffraction pattern of a sample obtained in Region D showed that it was a mixture of γ-Fe_2O_3 and α-Fe_2O_3. A broad maximum in the log σ vs. $1/T$ curve was observed between 390 and 450 °C. The

TABLE 4

X-ray diffraction data of Fe_3O_4 and FeO obtained from $FeC_3H_2O_4 \cdot 2H_2O$ by heating under dynamic air at 240 °C

Observed *d*-spacing values (present study) (Å)	Fe_3O_4 *d*-spacing values [18] (Å)	FeO (cubic) *d*-spacing values [17] (Å)	FeO (rhombohedron) *d*-spacing values [19] (Å)
(Å)			
2.978(m)	2.967(30) [a]		
2.531(s)	2.532(100)		
2.482(s)		2.49(80) [a]	
2.152(s)		2.153(100)	
2.089(w)	2.099(20)		
1.598(m)	1.616(30)		
			1.523(100)
			1.512(100)
1.523(m)		1.523(60)	
1.487(m)	1.485(40)		
1.300(w)		1.299(25)	1.301(20)

[a] Figures in parentheses show the relative line intensities, normalised to that of the strongest intensity line (given by 100).

conductivity measurements on the oxide obtained at 450 °C on cooling and reheating indicate the formation of α-Fe_2O_3; X-ray diffraction pattern analysis confirmed the formation of this phase.

Although the decomposition of $FeC_3H_2O_4 \cdot 2H_2O$ in static air and dynamic air followed a similar pattern, the formation of pure γ-Fe_2O_3 could not be obtained. Experimental investigations in dynamic air containing water vapour provided further information on the thermal decomposition of $FeC_3H_2O_4 \cdot 2H_2O$.

Dynamic air containing water vapour

The progress of the decomposition of $FeC_3H_2O_4 \cdot 2H_2O$ in dynamic air containing water vapour (Fig. 4), as studied by IR spectra, elemental analysis and XRD, indicated the formation of anhydrous malonate at 230 °C. There was a steep increase in the value of σ between 250 and 275 °C (Region B) followed by a decrease and then steep increase within the temperature range 275–308 °C (Region C of Fig. 4). Comparison of conductivity curves obtained in dynamic air and dynamic air containing water vapour indicated that the pattern of decomposition was not very different for the two environments. Temperatures for the formation of FeO and Fe_3O_4 were almost comparable. In addition, a definite well-resolved kink in the log σ vs. $1/T$ plot was observed between 308 and 322 °C in dynamic air containing water vapour (see Fig. 4). A careful analysis of the time-dependent σ measurements in this temperature range shows the following points:

(a) There is no change in the value of σ with time up to 316 °C.

(b) At 316 °C the specific conductivity changes from 10^{-5} ohm^{-1} cm^{-1} to 10^{-7} ohm^{-1} cm^{-1} within 18 min (see Fig. 5).

(c) There was no further decrease in values of σ above 316 °C.

(d) For the sample heated to 316 °C and then cooled, the log σ vs. $1/T$ curves for cooling and heating do not overlap; and the cooling curve was reasonably linear while the heating curve showed a definite maximum (Fig. 5).

The sample thus obtained was heated under nitrogen at 310 °C to remove any water. The X-ray diffraction pattern of this sample (Table 5) was very sharp indicating that the sample was highly crystalline, similar to results reported for γ-Fe_2O_3 [23]. At 340 °C in dynamic air containing water vapour, α-Fe_2O_3 was formed.

The analysis of the different paths of the decomposition of $FeC_3H_2O_4 \cdot 2H_2O$ in different atmospheres showed complete dehydration only under a dynamic dry nitrogen atmosphere, as was seen from thermal analysis, conductivity measurements and the shifts of malonate bands in the IR spectrum. A transformation of $FeC_3H_2O_4$ to FeO was detected. A separate phase of FeO could not be obtained, and it always occurred with $FeC_3H_2O_4$.

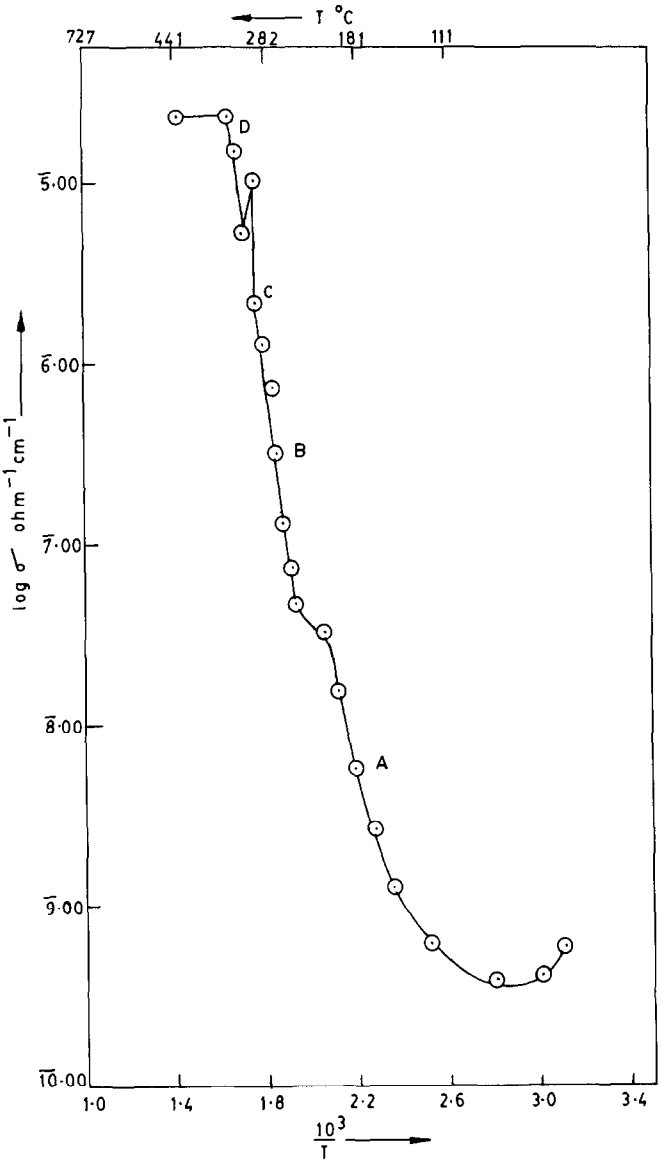

Fig. 4. Plot of log σ vs. $1/T$ of $FeC_3H_2O_4 \cdot 2H_2O$ decomposed under dynamic air containing water vapour.

This mixture of FeO and $FeC_3H_2O_4$ then transformed to Fe_3O_4 which is the final product obtained in dry nitrogen.

The decomposition paths of $FeC_3H_2O_4 \cdot 2H_2O$ in dynamic air, dynamic air containing water vapour, and static air were found to be similar except the step for the formation of the intermediate γ-Fe_2O_3. In dynamic air containing water vapour a separate step for the formation of pure γ-Fe_2O_3 was detected.

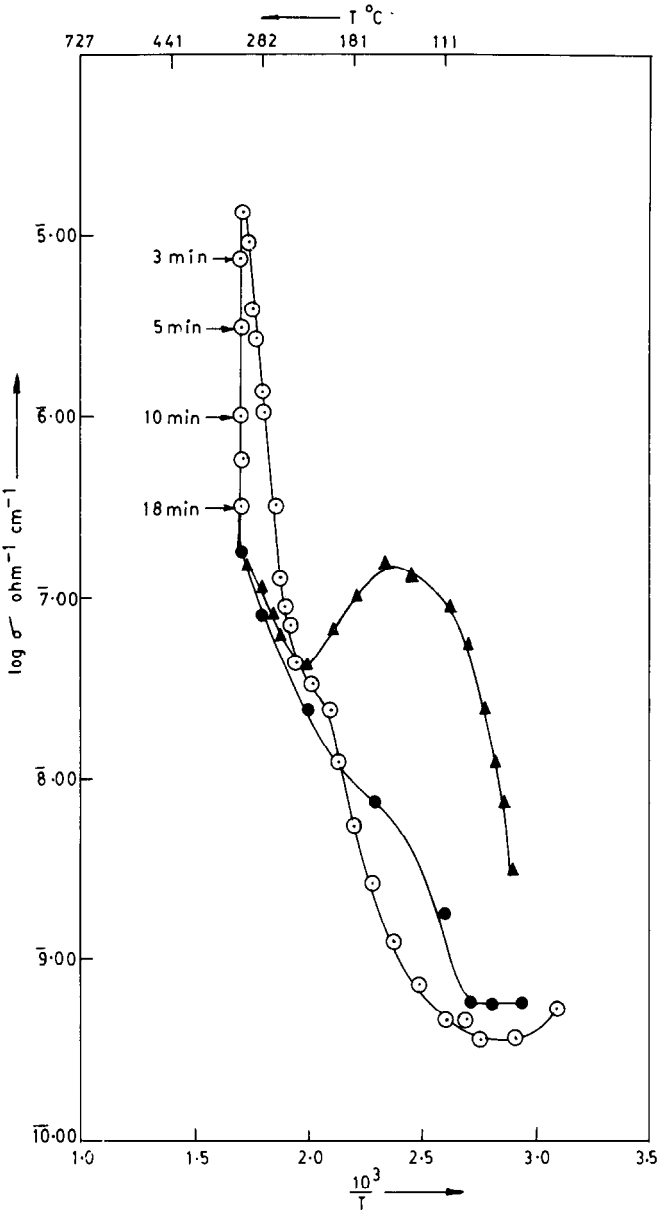

Fig. 5. Plot of log σ vs. $1/T$ of $FeC_3H_2O_4 \cdot 2H_2O$ during decomposition in dynamic air containing water vapour. ⊙, During decomposition; ●, cooling cycle for γ-Fe_2O_3; ▲, heating cycle for γ-Fe_2O_3.

The γ-Fe_2O_3 thus obtained in dynamic air containing water vapour showed that it has a coercive force of 275 Oe, saturation magnetisation of 69 emu g^{-1} and ratio of remanence to saturation magnetisation of 0.56 on magnetic hysteresis measurements. These values were comparable with those

TABLE 5

XRD data of γ-Fe_2O_3 obtained from ferrous malonate dihydrate by heating under dynamic air containing water vapour

Observed *d*-spacing values for γ-Fe_2O_3 (present study) (Å)	γ-Fe_2O_3 (tetragonal) *d*-spacing values [23] (Å)	γ-Fe_2O_3 (cubic) *d*-spacing values [24] (Å)
	7.91(1) [a]	
	6.94(2)	
5.90(2) [a]	5.90(6)	5.90(2) [a]
	5.33(1)	
4.84(4)	4.82(6)	4.82(5)
	4.29(2)	
4.18(2)		4.18(1)
3.73(5)	3.73(6)	3.73(5)
3.41(4)	3.40(7)	3.41(2)
	3.20(3)	
2.96(27)	2.95(30)	2.95(34)
2.78(16)	2.78(13)	2.78(19)
2.635(2)	2.638(4)	2.64(–)
2.52(100)	2.514(100)	2.52(100)
	2.408(2)	
2.33(5)	2.315(2)	2.32(6)
2.23(1)	2.23(2)	2.23(1)
2.09(20)	2.086(15)	2.08(24)
1.87(4)	1.865(1)	1.87(4)
	1.82(3)	
1.70(14)	1.701(19)	1.70(12)
	1.67(2)	
1.608(35)	1.604(20)	1.61(33)
1.55(2)	1.55(2)	1.55(<1)
1.53(1)	1.525(3)	1.53(1)
1.477(47)	1.474(40)	1.48(53)
1.43(1)		1.43(1)
1.32(5)	1.318(6)	1.32(7)
1.27(12)	1.272(8)	1.27(11)

[a] Figures in parentheses show the relative intensities normalised to that of the strongest intensity line (given by 100).

reported in refs. 8, 25 and 26. Since γ-Fe_2O_3 is ferrimagnetic, initial susceptibility measurements were employed to obtain the Curie temperature T_c. The χ_i–T measurements showed γ-Fe_2O_3 to be single domain with a well-defined Hopkinson peak [27] before its transformation to α-Fe_2O_3. The Curie temperature T_c for the transformation of γ-Fe_2O_3 to α-Fe_2O_3 occurred at 425 °C. The Mössbauer spectrum showed six well-resolved narrow bands (half line width 0.2285 mm) in the intensity ratio 3 : 2 : 1 : 1 : 2 : 3, and the value of the hyperfine field was found to be 498.5 $\pm$ 5.0 kOe, similar to that

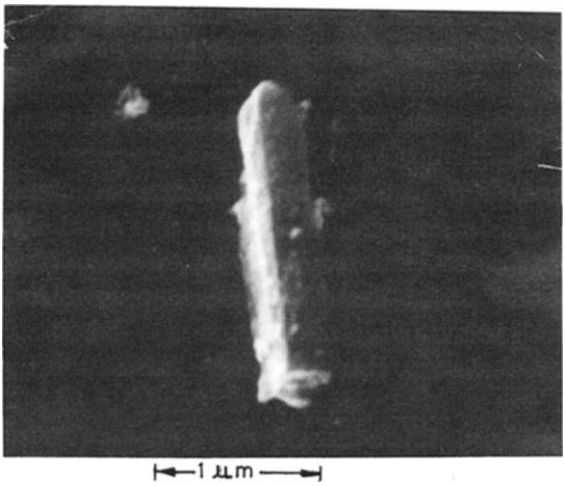

Fig. 6. SEM of a single γ-Fe_2O_3 particle.

reported in ref. 28. The SEM showed γ-Fe_2O_3 particles to be 1–2 μm in length with acicular shape (Fig. 6).

CONCLUSIONS

The present study suggested the following important points in the solid-state decomposition of $FeC_3H_2O_4 \cdot 2H_2O$:

(a) The TGA curve under dry nitrogen atmosphere showed a three-step decomposition, whereas in dynamic air and static air a continuous weight loss (one-step decomposition) was observed.

(b) The dehydration step of $FeC_3H_2O_4 \cdot 2H_2O$ yielding anhydrous $FeC_3H_2O_4$ was very clearly indicated only in dry nitrogen on the TGA curve.

(c) In dry nitrogen the log σ vs. $1/T$ plot showed a well-characterised step corresponding to dehydration. The formation of FeO as an intermediate was confirmed. FeO was always formed together with $FeC_3H_2O_4$.

(d) In dynamic air containing water vapour the exact conditions were determined by electrical conductivity measurements for obtaining pure γ-Fe_2O_3 (air flow 60–65 ml min^{-1}; temp. 315 °C; time 30 min; and water vapour obtained by passing air through a water bath controlled at 60–80 °C).

(e) The final product in dynamic air, dynamic air containing water vapour and static air was found to be α-Fe_2O_3, whereas in dry nitrogen it was found to be Fe_3O_4.

(f) The high field hysteresis loop (HLT), the χ_i–T measurements and the SEM showed that the γ-Fe_2O_3 sample synthesised from $FeC_3H_2O_4 \cdot 2H_2O$ possessed the properties required for an efficient tape-recording material.

ACKNOWLEDGEMENT

The authors are grateful for the financial assistance given by Grants-in-aid (Ministry of Defence), Government of India.

REFERENCES

1 R.M. White, J. Appl. Phys. 57 (1985) 2996.
2 M.P. Sharrock and R.E. Bodnar, J. Appl. Phys. 57 (1985) 3919.
3 D.J. Craik, Magnetic Oxides, Vol. 2, Wiley-Interscience, New York, 1975.
4 P.D. Pesher and O. Tsyrnorechki, Chem. Abstr., 55 (1961) 9137h.
5 O. Tsyrnorechki and I.V. Arshinar, Chem. Abstr., 55 (1961) 9138b.
6 V. Rao, A.L. Shashimohan and A.B. Biswas, J. Mater. Sci., 9 (1974) 430.
7 K. Seshan, H.R. Anantharaman, V. Rao, A.L. Shashimohan, H.V. Kheer and D.K. Chakraborty, Bull. Mater. Sci., 3a (1981) 201.
8 K.S. Rane, A.K. Nikumbh and A.J. Mukhedkar, J. Mater. Sci., 16 (1981) 2387.
9 J. Trau, J. Therm. Anal., 6 (1974) 355.
10 A. Venkataraman, V.A. Mukhedkar, M.M. Rahman, A.K. Nikumbh and A.J. Mukhedkar, Thermochim. Acta, 112 (1987) 231.
11 A. Venkataraman, V.A. Mukhedkar, M.M. Rahman, A.K. Nikumbh and A.J. Mukhedkar, Thermochim. Acta, 115 (1987) 215.
12 K. Muraishi, T. Takano, K. Nagase and N. Tanaka, J. Inorg. Nucl. Chem., 43 (1981) 2293.
13 K. Nagase, K. Muraishi, K. Sone and N. Tanaka, Bull. Chem. Soc. Jpn., 48 (1975) 3184.
14 A. Kwiatkowsky, J. Prezedmojsky and B. Pura, Mater. Res. Bull., 4 (1969) 765.
15 D.A. Deshpande, K.R. Ghormare, N.D. Deshpande and A.V. Tankhiwale, Thermochim. Acta, 62 (1983) 333.
16 N.T. McDevitt and W.L. Baun, Spectrochim. Acta, 20 (1964) 799.
17 ASTM File number 6-615.
18 ASTM File number 19-629.
19 ASTM File number 6-711.
20 C.A. Domencali, Phys. Rev., 78 (1950) 458.
21 B.A. Calhoun, Phys. Rev., 94 (1954) 1577.
22 P.A. Miles, W.B. Westphel and V. Von Hippel, Rev. Mod. Phys., 29 (1957) 279.
23 ASTM File number 25-1402.
24 ASTM File number 24-81.
25 G. Bate, in D.J. Craik (Ed.), Magnetic Oxides, Vol. 2, Wiley-Interscience, New York, 1975.
26 V. Rao, A.L. Shashimohan and A.B. Biswas, J. Mater. Sci., 9 (1974) 430.
27 C.R.K. Murty, J. Geol. Soc. Ind., 26 (1985) 640.
28 W.H. Kelly, V.J. Folen, M. Hass, W.N. Schreiner and G.B. Beard, Phys. Rev., 124 (1961) 80.